drones

MDPI

Article

Closed-Loop 3D Path Planning and Local Replanning for UAV Inspection in GIS Rooms

Xiaoyi Liu [1,†], Yuhan Yin [1,†], Kunxiao Wu [1], Yetong Zhang [1], Jianyong Zheng [1,*], Penghao Chen [1], Kangxin Cai [1] and Fei Mei [2]

[1] School of Electrical Engineering, Southeast University, Nanjing 210096, China; 220255278@seu.edu.cn (X.L.); yinyuhan@seu.edu.cn (Y.Y.); 220243168@seu.edu.cn (K.W.); 220255288@seu.edu.cn (Y.Z.); 220234999@seu.edu.cn (P.C.); 220245298@seu.edu.cn (K.C.)
[2] College of Energy and Electrical Engineering, Hohai University, Nanjing 211100, China; meifei@hhu.edu.cn
* Correspondence: jy_zheng@seu.edu.cn; Tel.: +86-183-6119-9298
† These authors contributed equally to this work.

Highlights

What are the main findings?

- A topology-and-corridor-guided bias-suppressed D* method (TCG-BS-D*) is developed for closed-loop 3D path planning and local replanning of UAV inspection missions in GIS rooms.
- The proposed method achieves the best overall balance of inspection efficiency, safety margin, trajectory regularity, and corridor consistency in static closed-loop inspection, with a 700.22 m path length, 269.32 s inspection time, an 8.18 m average safety clearance, 37 large-angle turns, and an 80.73% corridor adherence rate.

What are the implications of the main findings?

- The study shows that incorporating corridor topology and path regularization can improve the structural consistency and engineering executability of UAV inspection paths in confined indoor substation environments.
- The local replacement-based replanning strategy allows the inspection path to remain continuous and safe under maintenance blockage and dynamic disturbances, supporting more practical autonomous UAV inspection in GIS rooms.

Abstract

To address the problems of closed-loop task organization, strong corridor constraints, and path failure after local disturbances in unmanned aerial vehicle (UAV) inspection of gas-insulated switchgear (GIS) rooms, this paper proposes a topology-and-corridor-guided bias-suppressed D* (TCG-BS-D*) method for closed-loop three-dimensional (3D) path planning and local replanning. The proposed method constructs a structured guidance model based on the inspection-corridor topology, generates local 3D path segments according to a predetermined inspection sequence, and forms a nominal closed-loop inspection path through bias suppression and path regularization. Meanwhile, for local maintenance blockage and dynamic disturbance scenarios, an alternative local replanning strategy is applied to the affected path segments. Simulation results show that, under the static closed-loop inspection condition, the proposed method achieves a total path length of 700.22 m, a total inspection time of 269.32 s, an average safety clearance of 8.18 m, 37 large-angle turns, a corridor adherence rate of 80.73%, and a task completion rate of 100%, showing superior performance in inspection efficiency, safety margin, trajectory regularity, and corridor consistency. Under the local blockage condition, the replanned path introduces

Check for updates

Academic Editor: Octavio Garcia-Salazar

Received: 23 April 2026
Revised: 18 June 2026
Accepted: 20 June 2026
Published: 23 June 2026

Copyright: © 2026 by the authors. Licensee MDPI, Basel, Switzerland. This article is an open access article distributed under the terms and conditions of the Creative Commons Attribution (CC BY) license.

path-length and time increments of 71.29 m and 25.88 s, respectively, while maintaining the minimum safety clearance at 1.52 m and increasing the corridor adherence rate to 83.91%. Under dynamic disturbance conditions, the minimum dynamic safety clearance is improved from −2.71 m to 17.84 m, effectively eliminating the local dynamic collision risk. The results demonstrate that the proposed method can balance closed-loop path-generation efficiency, corridor-structure consistency, safety margin, and adaptability to local disturbances, providing an effective solution for UAV inspection path planning in GIS rooms.

Keywords: GIS room; UAV inspection; closed-loop 3D path planning; local replanning; corridor topology guidance; dynamic obstacle avoidance

1. Introduction

A gas-insulated switchgear (GIS) room is an important primary-equipment space in substations and converter stations, and the operating condition of the equipment inside directly affects the safe and stable operation of the power system. The main purpose of GIS room inspection is to acquire information on equipment appearance, connection components, cabinet conditions, support structures, and local abnormalities, thereby providing fundamental data for condition perception, defect identification, and intelligent operation and maintenance. With the increasingly compact arrangement of station equipment, the growing enclosed nature of indoor spaces, and the continuous increase in inspection frequency, traditional manual close-range inspection faces problems such as high safety risk, low inspection efficiency, and difficulty in accessing certain regions. Fixed cameras, online sensors, and local monitoring devices can continuously monitor key positions; however, their viewpoints and installation locations are relatively fixed and are easily blocked by cabinets, support structures, busbar connectors, and maintenance facilities. Therefore, it is difficult for fixed monitoring systems to fully cover the back side, top side, connection areas, and temporary focus regions of the equipment. Moreover, adding new fixed monitoring points is often constrained by construction space, wiring conditions, and outage arrangements, making it difficult to fully meet the needs of refined and mobile inspection. Therefore, without replacing fixed monitoring systems, introducing UAVs as mobile inspection platforms can provide flexible viewpoints, close-range observation, and sequential access capability, thereby effectively supplementing fixed monitoring blind spots.

In recent years, UAVs have rapidly developed in power infrastructure inspection and have shown great potential in transmission-line image detection, visual navigation, LiDAR perception, and autonomous inspection systems [1–5]. In power inspection applications, existing studies mainly focus on transmission lines, outdoor substation equipment, and large-scale energy facilities. Ref. [6] reviewed AI-based UAV inspection systems for power infrastructure, indicating that the combination of UAVs and intelligent perception technologies has become an important direction for power inspection. Ref. [7] developed an autonomous UAV inspection system for high-voltage transmission lines, and Ref. [8] applied target detection to correct transmission-line inspection, improving the automation and autonomy of line inspection tasks. However, these studies mainly focus on outdoor line-type tasks, where inspection objects are distributed along linear spaces, and the flight environment is relatively open. Their task organization differs significantly from the fixed-order, corridor-constrained, and closed-loop inspection requirements inside GIS rooms. Ref. [9] studied automated mission planning for thermal inspection in large power plants, and Ref. [10] summarized UAV inspection methods, challenges, and applications for power

lines. These studies provide important foundations for power inspection UAV applications, but GIS rooms still require further consideration of dense equipment arrangements, corridor accessibility, task visiting sequence, and local disturbance correction.

In terms of path-planning theory, traditional graph search, sampling-based planning, and local obstacle-avoidance methods provide important support for UAV 3D path generation. Ref. [11] reviewed UAV path planning and obstacle-avoidance algorithms, Ref. [12] compared representative sampling-based motion planning methods, Ref. [13] proposed the probabilistic roadmap method, and Ref. [14] established the theoretical foundation for sampling-optimal planners such as RRT*. These methods are highly general and suitable for ordinary free-space or point-to-point navigation tasks. However, in GIS room inspection, path planning is not merely to find the shortest connection between a start point and an end point. Instead, it needs to organize a closed-loop path around a fixed inspection sequence through the upper and lower equipment corridors and the middle connection corridor. If general free-space search methods are directly applied, the path may oscillate in the middle region, local connections may lack engineering interpretability, and corridor consistency may be insufficient, making the planned path difficult to execute and verify in indoor inspection.

Studies on local planning and 3D path generation in complex environments have also provided useful references. Ref. [15] investigated model-based UAV local path planning, Ref. [16] proposed a sparse-grid-based Lazy Theta* method for 3D planning, Ref. [17] incorporated a safety-enhancement mechanism into particle-swarm-based path planning, and Ref. [18] developed an energy-efficient 3D path-planning model for fixed-wing UAVs. These studies are valuable in terms of planning efficiency, local obstacle avoidance, and safety constraints. However, most of them still focus on point-to-point connectivity, single-task arrival, or obstacle avoidance in general 3D environments. They do not sufficiently model the organizational mode of visiting multiple bay task points and connection-area task points in a fixed sequence in the GIS room closed-loop inspection, nor do they fully exploit the stable prior of the internal corridor structure of GIS rooms.

UAV path planning under dynamic environments and complex constraints has also attracted increasing attention. Ref. [19] improved search efficiency in crowded environments using PF-RRT* and goal-bias strategies, Ref. [20] applied Q-learning to dynamic obstacle avoidance, Ref. [21] reviewed recent developments of RRT-based methods, Ref. [22] combined fluid-dynamic systems with neural networks for real-time 3D dynamic planning, Ref. [23] coupled path planning with tracking control, Ref. [24] studied optimal replanning for UAV collision avoidance, and Ref. [25] improved dynamic obstacle avoidance based on collision prediction. These studies improve the adaptability of path-planning methods to dynamic obstacles and local disturbances. However, most of them focus on general mobile obstacle avoidance or single-target arrival. In GIS room inspection, local blockage or short-term occupation of a corridor by personnel or mobile equipment usually affects only a local segment of the closed-loop inspection path. Replanning the entire closed-loop path after every disturbance would increase computational burden and may destroy the original inspection sequence and path-structure stability. Therefore, a more suitable strategy for GIS room inspection is to perform local alternative replanning only for the affected segment while preserving the global closed-loop task framework.

Studies on constrained corridor flight and high-voltage scenario safety constraints have shown that safety flight corridors can improve trajectory generation efficiency [26], A*-based methods can be improved by minimizing the number of turns [27], and safety-distance constraints can be incorporated into UAV inspection path planning in substation scenarios [28]. These studies indicate that safety margin, path smoothness, and corridor constraints are key factors affecting the engineering executability of UAV inspection in

constrained spaces. Nevertheless, existing studies have not formed a unified planning framework for GIS room closed-loop inspection tasks. In particular, the following issues remain insufficiently addressed: first, the closed-loop visiting relationship among fixed inspection sequence, bay task points, and connection-area task points is not sufficiently modeled; second, the corridor structure is not fully utilized to balance path efficiency and corridor consistency; third, the path correction mechanism under local maintenance blockage and dynamic disturbance is not sufficiently described; and fourth, although some methods can obtain short paths, their trajectory morphology has no clear correspondence with the actual passable corridors in GIS rooms, reducing engineering interpretability and subsequent execution stability.

To address these problems, this paper proposes a topology-and-corridor-guided bias-suppressed D* (TCG-BS-D*) method for closed-loop 3D path planning and local replanning. The proposed method is designed for GIS room inspection scenarios characterized by dense equipment, clear corridor structures, fixed task sequences, and possible local environmental disturbances. It takes the inspection-corridor topology as a structural prior, generates local 3D path segments according to the predetermined inspection sequence, and reduces unnecessary deviations and redundant turns through bias suppression and path regularization, thereby forming a nominal closed-loop inspection path with high corridor consistency and engineering executability. When a local maintenance blockage or dynamic obstacle disturbance occurs, the proposed method performs alternative replanning only for the affected segment while keeping the remaining path segments and the overall task sequence unchanged, thereby balancing path continuity, local adaptability, and closed-loop task stability.

The main contributions of this paper are as follows:

1. A 3D path-planning framework for closed-loop UAV inspection in GIS rooms is constructed. The framework jointly models bay inspection objects, connection-area inspection objects, the takeoff/landing point, and the fixed visiting sequence. Combined with the corridorized spatial structure of the GIS room, the inspection task is extended from general point-to-point path search to structured path planning with a clear visiting sequence and closed-loop constraints.
2. A TCG-BS-D* closed-loop 3D path-planning method is proposed. The method integrates corridor-topology guidance, closed-loop segment generation, bias suppression, and path regularization. It avoids path oscillation caused by unconstrained free-space search and reduces local redundant turns caused by excessive reliance on corridor graphs, enabling the generated path to balance inspection efficiency, corridor consistency, and flight executability.
3. A local alternative replanning mechanism for local maintenance blockage and dynamic obstacle disturbance is established. Without changing the overall inspection sequence or the closed-loop task framework, the mechanism locally repairs only the disturbed segment, improving the adaptability of GIS room inspection paths to temporarily inaccessible regions and dynamic corridor occupation.
4. A GIS room simulation scenario including static closed-loop inspection, local maintenance blockage, and dynamic obstacle disturbance is constructed. The effectiveness of the proposed method is verified in terms of total path length, inspection time, safety clearance, number of large turns, corridor adherence rate, and task completion rate, providing a reproducible simulation basis for UAV inspection path planning in GIS rooms.

2. Problem Description and Mathematical Formulation for UAV Inspection in GIS Rooms

2.1. Problem Description of Closed-Loop Inspection

This paper investigates the closed-loop path-planning problem for UAV inspection in GIS rooms. Different from general free-space path planning, this problem has the following characteristics. First, the inspection targets are fixed in position, and the visiting order is predefined. Second, the flight environment is constrained by equipment, cabinets, supporting components, and connection structures, which constitute a typical confined 3D space. Third, most effective flight segments exhibit evident corridor-like characteristics. Therefore, the planned path should not only satisfy reachability and obstacle-avoidance requirements, but also conform, as much as possible, to the structural distribution of indoor inspection corridors.

Let the 3D workspace of the GIS room be denoted by

$$\Omega \subset \mathbb{R}^3 \tag{1}$$

The UAV departs from the takeoff-and-landing point S, sequentially visits the bay inspection targets and connection-area inspection targets, and finally returns to S, thereby forming a closed-loop inspection mission. For unified modeling, all inspection targets are represented by the task set

$$Q = \{S, B_1, B_2, \ldots, B_{N_b}, C_1, C_2, \ldots, C_{N_c}\} \tag{2}$$

where B_i denotes the i-th bay inspection task target; C_j denotes the j-th connection-area inspection task target.

It should be noted that the term *bay* in this paper does not refer to a single geometric component, but to an inspection task unit. At the path-planning level, independent tasks are not assigned to each individual local device. Instead, the major inspection requirements around the same functional location are merged into one bay inspection target. In this way, the inspection problem in a GIS room is formulated as a closed-loop path-planning problem involving the sequential visit of multiple task units in a fixed order. The purpose of this treatment is to emphasize the characterization of the inspection process and visiting sequence at the path-planning level, rather than to model each device in detail.

It should be further clarified that bay inspection objects and connection-area inspection objects are both task points at the path-planning level, but they have different engineering meanings. Bay inspection objects mainly correspond to GIS bay units and nearby main equipment and are usually distributed near the upper and lower rows of main equipment. Connection-area inspection objects correspond to busbar connection sections, transverse connection structures, or corridor-switching areas. Their role is not only to complete local equipment-state inspection, but also to connect the upper and lower inspection corridors and maintain the continuity of the closed-loop inspection path. Therefore, connection-area task points have both inspection-target and path-transition attributes in the task sequence.

In addition, the closed-loop path-planning problem studied in this paper is based on the task-reachability assumption. That is, each inspection object has at least one reachable access region that is not completely blocked, and this access region is connected to the main inspection corridor topology of the GIS room. If a task object is completely enclosed by obstacles, maintenance facilities, or other temporary restricted regions, causing its access region to be completely disconnected from the feasible flight space, then the problem is no longer a local path-replanning problem. Instead, the task layer should reschedule the inspection sequence, wait for site recovery, or trigger manual intervention. The subsequent

algorithm and simulations in this paper are conducted under the condition that task objects are not completely blocked and that at least one feasible corridor exists.

Let the prescribed inspection sequence be

$$\Pi = \{q_0, q_1, \ldots, q_M\} \tag{3}$$

where $q_0 = q_M = S$, and the intermediate elements represent the bay and connection-area task targets arranged in the predefined order. The objective of this paper is to generate a closed-loop 3D inspection path that completes the sequence Π while satisfying obstacle-avoidance, safety, and flight-executability constraints.

2.2. 3D Obstacle Modeling in GIS Rooms

Objects inside a GIS room are generally regular in shape, making them suitable for geometric approximation in obstacle modeling. To balance modeling accuracy and collision-detection efficiency, this paper uses two basic geometric primitives, namely cuboids and cylinders, to represent the main indoor obstacles.

Let the set of cuboid obstacles be denoted by

$$O_b = \left\{ o_b^1, o_b^2, \ldots, o_b^{N_b} \right\} \tag{4}$$

where an arbitrary cuboid obstacle is defined as

$$o_b^i = (x_i, y_i, z_i, l_i, w_i, h_i) \tag{5}$$

where (x_i, y_i, z_i) denotes the obstacle-center coordinate; l_i, w_i, and h_i denote its dimensions along the x-, y-, and z-directions, respectively.

Let the set of cylindrical obstacles be denoted by

$$O_c = \left\{ o_c^1, o_c^2, \ldots, o_c^{N_c} \right\} \tag{6}$$

An arbitrary cylindrical obstacle is defined as

$$o_c^j = (x_j, y_j, z_j, L_j, r_j, d_j) \tag{7}$$

where (x_j, y_j, z_j) denotes the reference center of the cylinder; L_j denotes the axial length; r_j denotes the radius; $d_j \in \{x, y, z\}$ denotes the principal axis direction of the cylinder.

Accordingly, the overall obstacle set in the scene can be written as

$$O = O_b \cup O_c \tag{8}$$

Considering the UAV body size, modeling errors, and flight safety margin, a unified safety inflation radius, r_s, is adopted to inflate the obstacles. The inflated obstacle set is denoted by O^+.

On this basis, the feasible flight region for the UAV inside the GIS room is defined as

$$F = \Omega \backslash O^+ \tag{9}$$

The advantage of this modeling approach is twofold. On the one hand, it preserves the spatial structural characteristics of equipment layout in the GIS room. On the other hand, it facilitates the subsequent construction of unified collision-detection and local-replanning criteria.

2.3. Task Visiting and Path Representation

Let the closed-loop inspection path of the UAV consist of a set of discrete trajectory points, denoted by

$$P = \{p_0, p_1, \ldots, p_N\} \tag{10}$$

where

$$p_k = (x_k, y_k, z_k) \in F, \quad k = 0, 1, \ldots, N. \tag{11}$$

The start point and end point of the path both correspond to the takeoff-and-landing point S.

To determine whether the UAV has visited a task target, an access region A_i is defined for each task target q_i. Once the path enters A_i, the corresponding inspection visit is regarded as completed. Therefore, the task-visiting constraint can be written as

$$P \cap A_i \neq \varnothing, \quad i = 1, 2, \ldots, M-1. \tag{12}$$

Meanwhile, to ensure the correctness of the task order, the visiting order of the access regions along the path should be consistent with the inspection sequence Π. That is, if q_i precedes q_j in the sequence, then the first time at which the path enters A_i should be earlier than that at which it first enters A_j.

For collision avoidance, the line segment between any two adjacent trajectory points must lie entirely within the feasible region, namely

$$\overline{p_k p_{k+1}} \subseteq F, \quad k = 0, 1, \ldots, N-1. \tag{13}$$

2.4. Flight Constraint Modeling

To improve the engineering executability of the planned path, in addition to collision-avoidance and task-visiting constraints, the altitude and turning-angle constraints of UAV flight in the GIS room should also be considered.

2.4.1. Altitude Constraint

Let the allowable flight-altitude range be $[z_{\min}, z_{\max}]$. Then any trajectory point on the path should satisfy

$$z_{\min} \leq z_k \leq z_{\max}, \quad k = 0, 1, \ldots, N. \tag{14}$$

2.4.2. Turn-Angle Constraint

To suppress sharp turns in the path, the direction vectors of two adjacent path segments are defined as

$$v_k = p_k - p_{k-1}, \quad v_{k+1} = p_{k+1} - p_k \tag{15}$$

Then, the turning angle at the k-th waypoint is given by

$$\theta_k = \arccos\left(\frac{v_k^T v_{k+1}}{\|v_k\| \|v_{k+1}\|}\right) \tag{16}$$

If θ_k is excessively large, and a significant turn exists at that point, which is unfavorable for stable UAV flight in narrow indoor corridors. Therefore, the occurrence of large turning angles should be suppressed as much as possible during path planning.

2.5. Simplified UAV Kinematic Model and Waypoint-Following Constraints

The inspection platform considered in this paper is a small multi-rotor UAV. This type of UAV has hovering capability, low-speed flight capability, and good spatial maneuverability, making it suitable for indoor inspection tasks in GIS rooms, where the space is

constrained, the corridors are narrow, and close-range observation is required. Since this paper focuses on task-level 3D path planning and local replanning rather than low-level flight-controller design, a simplified 3D kinematic model is adopted to describe the flight process of the UAV along the planned waypoint sequence.

Let the UAV position at time t be

$$p(t) = [x(t), y(t), z(t))^T \tag{17}$$

The kinematic relationship is expressed as

$$\dot{p}(t) = v(t) \tag{18}$$

where $v(t)$ is the UAV velocity vector. To ensure the basic flight executability of the planned path, the UAV flight speed should satisfy

$$\|v(t)) \leq v_{max} \tag{19}$$

The altitude and turn-angle constraints are described in Section 2.4. At the path-execution level, a waypoint-following assumption is adopted. That is, the UAV flies sequentially along the planned discrete trajectory points, and adjacent trajectory points are connected by piecewise linear segments. For any connection segment between two adjacent waypoints, collision constraints, safety-clearance constraints, altitude constraints, and turn-angle constraints must be satisfied. If a candidate connection segment violates any of these constraints, the segment is considered infeasible and must be regenerated or replaced through local replanning.

It should be noted that this paper does not focus on a specific localization algorithm or low-level attitude controller. Instead, it assumes that the UAV can obtain its pose, the static obstacle map, and local dynamic obstacle information through indoor localization and environmental perception modules. This assumption can correspond to practical systems based on LiDAR, vision, or UWB/LiDAR fusion localization and mapping. The focus of this paper is the 3D path organization, corridor-constraint utilization, and local path correction mechanism for closed-loop UAV inspection in GIS rooms.

2.6. Definition of Optimization Objectives

For the closed-loop inspection task in a GIS room, the optimization objectives include the total path length Ltotal, total inspection time Ttotal, minimum safety clearance Dmin, average safety clearance Davg, number of large-angle turns Nturn, corridor adherence rate Rcorr, and task completion rate CR.

2.6.1. Total Path Length

The total path length of the closed-loop path is defined as

$$L_{\text{total}} = \sum_{k=0}^{N-1} \|p_{k+1} - p_k\| \tag{20}$$

2.6.2. Total Inspection Time

Let the nominal cruising speed of the UAV be v. Then, the total inspection time can be expressed as

$$T_{\text{total}} = \frac{L_{\text{total}}}{v} \tag{21}$$

2.6.3. Minimum Safety Clearance

The minimum distance between the path and the inflated obstacle set is defined as

$$D_{\min} = \min_{p \in P} d\left(p, O^{+}\right) \tag{22}$$

where $d(\cdot)$ denotes the minimum Euclidean distance from a point to the obstacle set.

2.6.4. Average Safety Clearance

Based on the original minimum safety clearance Dmin, the average safety clearance Davg is further introduced to avoid relying only on a single closest point to evaluate path safety. Davg is used to characterize the overall safety margin of the entire path relative to the obstacle set. Suppose the path contains N discrete trajectory points, and the minimum Euclidean distance from path point pk to the inflated obstacle set O+ is d(pk, O+). Then the average safety clearance is defined as.

Where Dmin reflects the safety margin at the most dangerous position along the path, while Davg reflects the average distance between the entire path and the obstacles. Using both metrics provides a more comprehensive evaluation of path safety.

$$D_{avg} = \frac{1}{N} \sum_{k=1}^{N} d \tag{23}$$

2.6.5. Number of Large-Angle Turns

Given a turning-angle threshold θ_0, the number of large-angle turns is defined as

$$N_{turn} = \sum_{k=1}^{N-1} I(\theta_k > \theta_0) \tag{24}$$

where $I(\cdot)$ denotes the indicator function.

2.6.6. Corridor Adherence Rate

Let the total number of path points be N_all, where N_in denotes the number of path points located inside the valid corridor band and N_out denotes the number of path points outside the corridor band.

$$N_{all} = N_{in} + N_{out} \tag{25}$$

Then, the corridor adherence rate is defined as the proportion of path points located inside the valid corridor band and is expressed in percentage form as

$$R_{corr} = \frac{N_{in}}{N_{all}} \times 100\% \tag{26}$$

where the valid corridor band is jointly determined by the main inspection corridor centerlines and the corridor tolerance δ_corr. Compared with a decimal expression, a percentage expression more intuitively reflects the degree of path adherence to the existing inspection corridors in the GIS room. The number of in-corridor and out-of-corridor path points is also used in the replanning analysis to explain the variation of corridor adherence rate.

2.6.7. Task Completion Rate

Let the total number of tasks be $M - 1$, and the actual number of completed tasks is M_c. Then,

$$CR = \frac{M_c}{M - 1} \tag{27}$$

In summary, the closed-loop inspection path-planning problem in a GIS room considered in this paper can be stated as follows: under collision-avoidance, task-order, and flight constraints, generate a closed-loop 3D inspection path with a shorter total path length, lower total inspection time, larger safety margin, fewer large-angle turns, and a higher corridor adherence rate.

3. TCG-BS-D* Method for Closed-Loop 3D Path Planning and Local Replanning

3.1. Overall Framework of the Method

Considering the characteristics of GIS room inspection, including clear corridor structures, fixed-task visiting sequence, and possible local path failure caused by environmental changes, this paper proposes a topology-and-corridor-guided bias-suppressed D* (TCG-BS-D*) method for closed-loop 3D path planning and local replanning. The method does not adopt a one-shot global search strategy in completely free space. Instead, it uses the stable inspection corridors, clear task sequence, and usually limited local disturbance range in GIS rooms to decompose the closed-loop inspection path generation process into four stages: topology guidance, closed-loop segment generation, bias suppression and path regularization, and local alternative replanning.

Under nominal operating conditions, TCG-BS-D* first establishes a topological guidance model according to the inspection corridors and their connectivity, so as to reduce redundancy in continuous-space search. It then generates local 3D trajectories segment by segment between adjacent task targets according to the prescribed inspection sequence, and concatenates them into an initial closed-loop path. On this basis, local deviations and redundant turns in the path are regularized to make the resulting trajectory better conform to the structured inspection corridors in the GIS room. When a local area becomes impassable due to maintenance blockage or dynamic disturbances, the algorithm replans only the affected flight segment while keeping all unaffected path segments unchanged, thereby preserving the stability of the overall closed-loop inspection framework.

It should be noted that the "D*" in the proposed method is mainly reflected in the local cost-update and affected-segment replanning mechanism after local environmental changes. Unlike recomputing the entire global path, TCG-BS-D* marks only the affected local edge or path segment near the detected local obstacle or dynamic conflict as blocked or high-cost, and then searches for an alternative connection in the neighboring topology subgraph and local continuous space. This idea is consistent with the local incremental correction philosophy of D*/D* Lite methods in dynamic environments. However, the proposed method does not directly apply standard D* Lite as a complete global planner. Instead, it embeds the local correction idea into the topology-corridor framework for GIS room closed-loop inspection. Therefore, the core of TCG-BS-D* is not to pursue a geometrically shortest path, but to generate a structured closed-loop inspection path under the joint influence of task sequence, corridor structure, safety constraints, and local repairability.

3.2. Construction of the Topological Guidance Model

Most effective flight segments inside a GIS room follow existing inspection corridors. If this structural characteristic is ignored and a global search is directly performed in continuous 3D space, the result may suffer from excessive search redundancy, pronounced local oscillations, and limited interpretability. Therefore, TCG-BS-D* first constructs a topological graph according to the inspection corridors and their connectivity.

$$G = (V, E) \tag{28}$$

where V denotes the node set, and E denotes the edge set.

In this topological graph, nodes represent positions that are structurally meaningful for path connectivity, while edges describe the admissible passage relationships between these positions. For any edge $e_{ij} \in E$, let its geometric length be l_{ij}. If edge weights are determined solely by length, the graph-search result is mainly driven by geometric distance and cannot adequately reflect the requirements of corridor adherence and local regularity in UAV inspection paths for GIS rooms. To address this issue, a corridor-switching cost and a direction-change cost are further introduced in addition to the basic length term, and the comprehensive edge-cost function is defined as

$$J_{ij} = w_1 l_{ij} + w_2 s_{ij} + w_3 t_{ij} \tag{29}$$

where sij denotes the additional cost caused by corridor switching; tij denotes the additional cost caused by direction change; wl, ws, and wt are the corresponding weighting coefficients for the length term, corridor-switching term, and direction-change term, respectively. Their specific values are given in the experimental parameter table.

The above edge-cost design enables the topological search result to go beyond merely pursuing the geometrically shortest connection, and instead preferentially preserves structured connections that follow the main inspection corridors, involve fewer corridor switches, and exhibit smoother direction changes. Specifically, even if a candidate edge is relatively short, its overall cost will increase accordingly if it induces additional corridor switching or significant directional deviation. In contrast, candidate connections that extend along existing inspection corridors are more likely to be retained. In this way, the topological graph not only describes reachability relationships but also imposes structural constraints on the overall path morphology at the early stage of path generation.

Another role of the topological guidance model is to provide a unified basis for local replanning. When a local region is disturbed, it is unnecessary to perform a complete re-search over the entire global space. Instead, it is sufficient to search for an alternative connection on the topological subgraph near the disturbed region. This property allows TCG-BS-D* to maintain good computational efficiency and path continuity under local environmental changes.

3.3. Closed-Loop Path Segment Generation

After the topological guidance model is established, TCG-BS-D* decomposes the closed-loop task, according to the prescribed inspection sequence, into a set of local connection problems between adjacent task targets. For any pair of adjacent task targets, a reference node sequence is first obtained by searching on the topological graph G:

$$\Gamma_{i,i+1} = \{v_1, v_2, \ldots, v_n\} \tag{30}$$

This sequence provides the initial routing of the corresponding local flight segment in the structured corridor network. Subsequently, this reference connection is refined in continuous 3D space to generate a local 3D trajectory that satisfies the feasible-region constraints, task-visiting constraints, and flight constraints.

This "topological guidance–continuous refinement" strategy strikes a balance between structural prior information and geometric flexibility. At the topological level, a coarse path framework consistent with the inspection characteristics of GIS rooms can be obtained efficiently, thereby avoiding large-scale blind search in continuous space. The subsequent continuous-space refinement retains sufficient geometric freedom, allowing each local flight segment to adapt to the actual equipment layout and feasible-region boundary constraints, thus ensuring the geometric executability of the path.

After all local flight segments are generated, TCG-BS-D* concatenates them head to tail according to the inspection sequence to obtain an initial closed-loop inspection path. Since the entire path-generation process always follows the prescribed task-visiting order, the concatenated result naturally satisfies the organizational requirement of the closed-loop task. Meanwhile, the segment-wise construction manner also facilitates subsequent local replanning: when a local region is disturbed, only the corresponding local flight segment needs to be identified and replaced, rather than reconstructing the entire path.

It should be noted that, although the initial closed-loop path already possesses basic geometric feasibility and task completeness, a certain degree of local deviation and redundant turning may still exist near task-access segments, connection-area visiting segments, and cross-corridor switching segments. Therefore, further path regularization is still required to improve its structural quality.

3.4. Bias Suppression and Path Regularization

Although the initial closed-loop path completes all task connections, it may still contain problems such as local oscillations, redundant deviations in access segments, and unnecessary turns. If it is directly used as the final inspection path, the structural consistency and flight executability of the path may be compromised. To address this issue, TCG-BS-D* further performs bias suppression and regularization after the closed-loop path is generated.

First, to strengthen the path adherence to inspection corridors, the cumulative deviation cost of the path with respect to the inspection corridors is defined as

$$J_{dev} = \sum_{k=0}^{N} d(p_k, R) \tag{31}$$

where $d(p_k, R)$ denotes the distance from path point p_k to the nearest inspection corridor. A smaller J_{dev} indicates that the path is, as a whole, closer to the existing inspection corridors and therefore exhibits stronger structural consistency. By uniformly suppressing this quantity, ineffective deviations in the central region and local access segments can be effectively reduced, so that the overall path configuration better conforms to the structural characteristics of GIS-room inspection.

Second, to reduce redundant turns in the path, TCG-BS-D* regularizes nearly collinear segments and ineffective turning segments. For consecutively nearly collinear trajectory points, the intermediate redundant points are directly removed. For local flight segments with excessively frequent direction changes, the turning complexity is reduced by replacing the connection pattern or adjusting the access direction. The definition of the turning angle is not repeated here; instead, the large-angle-turn metric established earlier is directly used to control path turning complexity.

By comprehensively considering the total path length, cumulative deviation cost, and number of large-angle turns, the following global evaluation function is adopted to uniformly regularize the closed-loop path:

$$J(P) = \alpha L_{total}(P) + \beta J_{dev}(P) + \gamma N_{turn}(P) \tag{32}$$

where α, β, and γ are weighting coefficients. Since the total inspection time is linearly consistent with the total path length when the nominal cruising speed is given, the path generation and regularization stages mainly use L_total as the primary efficiency indicator, while T_total is evaluated uniformly in the experimental analysis.

It should be emphasized that bias suppression is not equivalent to simply "straightening" the path, and it does not allow the path to pass through obstacles. For any intermediate-

point removal or local-segment replacement, the algorithm rechecks feasibility. A regularization operation is accepted only when the candidate segment remains inside the feasible flight domain, satisfies the safety-clearance constraint with respect to the inflated obstacle set, respects the altitude limits, and does not introduce an excessive turn angle. If the candidate segment collides with obstacles, violates altitude limits, or introduces an excessive turn angle, the operation is directly rejected, and the original feasible segment is retained. Therefore, bias suppression reduces unnecessary deviations and redundant turns within the safety-feasible space rather than pursuing an unconstrained geometric straight line.

3.5. Local Replanning Mechanism

During actual inspection, local regions may become impassable due to maintenance operations, temporary blockage, or dynamic disturbances. If the entire closed-loop path were recomputed after each local disturbance, the computational burden would increase, and the overall structural stability of the existing path would also be compromised. To address this issue, TCG-BS-D* adopts a local replacement-based replanning strategy, in which only the affected flight segment is modified.

Let the nominal closed-loop path be denoted by P, and let the locally disturbed region be denoted by Z. If a local flight segment $P_{a,b}$ in the path conflicts with the disturbed region, i.e.,

$$P_{a,b} \cap Z \neq \varnothing. \tag{33}$$

Then local replanning is triggered. The algorithm marks the edge or segment intersecting Z as unavailable or high-cost and searches for an alternative connection in the topology subgraph near the disturbed region. The updated closed-loop path can be written as

$$P' = P_{before} \cup P'_{a,b} \cup P_{after} \tag{34}$$

where P_before and P_after are the unaffected path parts before and after the disturbed segment, respectively, and P′_{a,b} is the regenerated alternative segment. Thus, local replanning only modifies the disturbed local segment without changing the overall inspection sequence or the closed-loop task structure.

For the maintenance blockage scenario, the disturbed region Z can be regarded as a temporary static obstacle. In this case, the objective of local replanning is to bypass the blocked region without changing the original inspection sequence, and to reconnect to the original path within a local neighborhood. To this end, TCG-BS-D* searches for an alternative connection on the topological subgraph adjacent to the disturbed region, and then generates a new local 3D trajectory in continuous space. Since the unaffected preceding and succeeding path segments remain unchanged, the overall closed-loop inspection framework can still maintain good stability.

For the dynamic disturbance scenario, the disturbed region corresponds to a time-varying local conflict region. Let the center position of the dynamic obstacle be z_d(t), the safety radius of the dynamic obstacle be r_d, and the UAV safety radius be r_u. The occupied region of the dynamic obstacle is expressed as

$$O_d(t) = \{x \| \|x - z_d(t)) \leq r_d + r_u) \tag{35}$$

The dynamic safety clearance between path point p(t) and the dynamic obstacle is defined as

$$D_{dyn}(t) = \|p(t) - z_d(t)) - r_d - r_u \tag{36}$$

When D_dyn(t) is lower than the given safety threshold d_safe, the current segment is considered to have a dynamic conflict risk, and local replanning is triggered. If D_dyn(t) < 0,

then the UAV safety envelope overlaps with the occupied region of the dynamic obstacle, indicating a collision risk rather than a negative physical distance. In this case, TCG-BS-D* temporarily switches the UAV to an adjacent safe corridor through alternative corridor selection and local connection reconstruction, and then returns to the original inspection process after bypassing the dynamic obstacle.

To avoid deadlock in local alternative search, a hierarchical handling mechanism is adopted. First, an alternative connection is searched within the neighborhood of the disturbed segment. If no feasible segment exists in the local neighborhood, the search range is expanded to adjacent corridor nodes and upstream/downstream task-connection segments. If no path satisfying collision, safety-clearance, and turn-angle constraints can be found after expansion, the current task segment is considered temporarily infeasible, and hovering, returning to the previous safe waypoint, or task-layer replanning is triggered. The simulation in this paper is based on the condition that task objects are not completely blocked and that at least one feasible alternative corridor exists; therefore, local replanning can obtain feasible alternative segments.

3.6. Method Attributes and Safety Feasibility

In summary, TCG-BS-D* differs significantly from ordinary shortest-path search. Ordinary shortest-path search usually takes the minimum distance as the primary objective and focuses on connectivity between the start point and the end point. In contrast, the proposed method is designed for closed-loop inspection in GIS rooms and is constrained by a fixed visiting sequence, corridor topology, obstacle inflation, safety clearance, altitude range, turn-angle constraints, and local repairability. Its path-generation result is not solely determined by geometric distance, but is a closed-loop inspection trajectory formed under structured corridor priors and flight-executability constraints.

Topology guidance determines which inspection corridors the path should primarily follow. Closed-loop segment generation ensures task sequence and path continuity. Bias suppression reduces unnecessary deviations and redundant turns within the safety-feasible space. Local replanning replaces affected path segments when maintenance blockage or dynamic disturbance occurs. These components jointly improve corridor consistency, regularity, and local adaptability without damaging the task sequence. Therefore, the innovation of TCG-BS-D* lies not in simply shortening the path, but in integrating the corridor structure, closed-loop inspection sequence, and local disturbance correction mechanism specific to GIS rooms into a unified 3D path-planning framework.

4. Experimental Simulation and Results Analysis

4.1. GIS Room Inspection Scenario and Experimental Setup

To verify the applicability of the proposed method in an engineering scenario, the simulation scenario in this paper is derived from the spatial layout of an actual GIS room in Jiangsu Province, China. Considering the engineering sensitivity of on-site equipment information and station layout details, the actual station name and complete equipment parameters are not disclosed. Instead, the real GIS room is anonymized and geometrically abstracted while preserving the main spatial scale, equipment arrangement, corridor distribution, and inspection-task organization. Specifically, the scenario preserves key structural features such as the upper and lower rows of main GIS equipment, control cabinets, support columns, busbar connection structures, transverse connection sections, and inspection corridors between equipment. Regular equipment shapes are abstracted as cuboids and cylinders to meet the needs of path-planning simulation and collision checking.

The simulated GIS room space is 200 m $\times$ 100 m $\times$ 50 m. The equipment arrangement forms three main inspection corridors: the lower corridor, the middle corridor, and the

upper corridor. Their centerlines are y = 34 m, y = 50 m, and y = 66 m, respectively. These three corridors jointly form the main passable framework for closed-loop UAV inspection in the GIS room. Unlike a completely idealized indoor simulation environment, the task-point arrangement, corridor connections, and local blockage positions in this scenario refer to possible equipment occlusion, corridor restrictions, and local maintenance operations encountered during actual GIS room inspections.

As Figure 1 shows, in the task setting, 17 task points are arranged, including one takeoff/landing point, 12 bay inspection points, and 4 connection-area inspection points. The takeoff/landing point S is located in the middle corridor. The lower-row bay inspection points are denoted as B1-B6, the upper-row bay inspection points are denoted as B7-B12, and the connection-area inspection points are denoted as C1-C4. The closed-loop inspection task starts from S, sequentially visits all bay inspection points and connection-area inspection points, and finally returns to S. To improve the independent readability of the table, Table 1 supplements the visiting sequence based on the original coordinate information, thereby clarifying the execution process of the closed-loop inspection task.

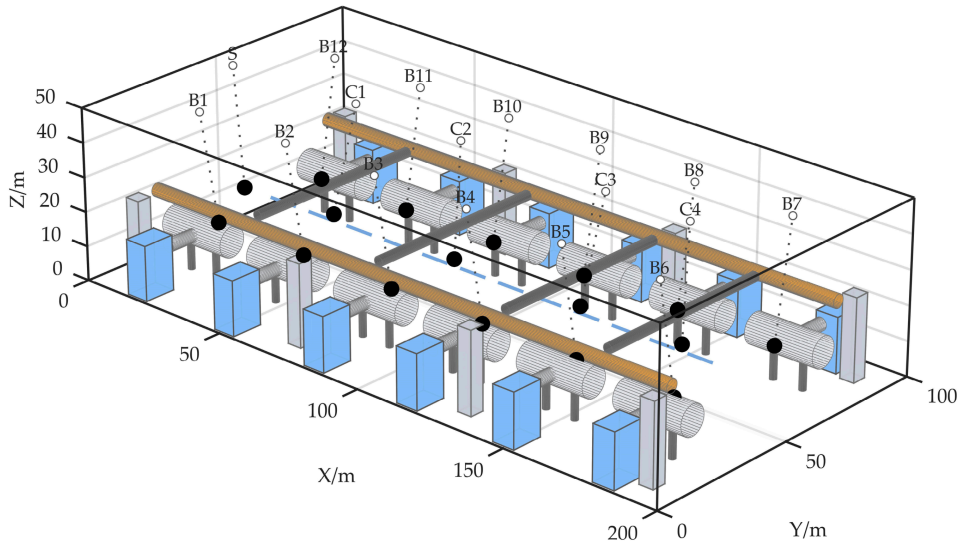


Figure 1. GIS-room inspection scenario and distribution of inspection task points.

Table 1. Inspection task points and visiting sequence in the GIS room.

Z/m	*Y*/m	*X*/m	Type	Task Point
14	50	10	start	S
13	30	20	bay	B1
13	30	52	bay	B2
13	30	84	bay	B3
13	30	116	bay	B4
13	30	148	bay	B5
13	30	180	bay	B6
13	70	180	bay	B7
13	70	148	bay	B8
13	70	116	bay	B9
13	70	84	bay	B10
13	70	52	bay	B11
13	70	20	bay	B12
16	50	44	conn	C1
16	50	88	conn	C2
16	50	132	conn	C3
16	50	166	conn	C4

A 3D GIS room simulation program is developed in MATLAB R2025a. The program first generates a 3D geometric scenario according to the anonymized real GIS room scale, equipment arrangement, and corridor structure. Then, a 3D occupancy grid is constructed with a fixed resolution, and obstacle safety inflation is performed. Finally, different path-planning methods are executed to obtain the corresponding closed-loop inspection paths and evaluation metrics. In the simulation, the UAV adopts the simplified kinematic model of the small multi-rotor UAV described in Section 2.5 and follows the planned waypoint sequence using piecewise linear tracking. To ensure fair comparison, all methods are run under the same scenario, task points, obstacle inflation radius, cruise speed, and evaluation metrics. For comparison methods involving random sampling, fixed random seeds are used.

The key simulation parameters and TCG-BS-D* method parameters are shown in Table 2. The scenario size, corridor centerlines, and task-point arrangement are derived from the geometrically abstracted actual GIS room. The nominal UAV cruise speed and cruise altitude are set according to the requirements of indoor low-speed inspection and passable corridor space. The safety inflation radius considers the UAV body envelope, modeling error, and localization-error margin. The corridor tolerance is used to determine whether a path point is located within the valid inspection corridor range. The large-turn threshold is used to evaluate the trajectory executability of the UAV in narrow corridors. The length, weight, corridor-switching weight, turn-penalty weight, and corridor-deviation weight of TCG-BS-D* are determined through preliminary experiments and kept unchanged in the static inspection, local blockage, and dynamic disturbance scenarios to avoid scenario-specific tuning.

Table 2. Key simulation and TCG-BS-D* parameter settings.

Parameter Category	Parameter	Value
Scenario source	GIS room scenario	Anonymized abstract scenario derived from an actual GIS room in Jiangsu Province, China
Scenario parameter	Simulation space size	200 m × 100 m × 50 m
Scenario parameter	Grid resolution	1.0 m
Scenario parameter	Main inspection corridor centerlines	y = 34 m, 50 m, 66 m
UAV parameter	UAV type	Small multi-rotor UAV
UAV parameter	Nominal cruise altitude	14 m
UAV parameter	Nominal cruise speed	2.6 m/s
Safety and constraint parameter	Obstacle safety inflation radius	3.4 m
Safety and constraint parameter	Corridor tolerance δ_{corr}	3.0 m
Safety and constraint parameter	Large-turn threshold θ_{max}	35°
TCG-BS-D* parameter	Length weight w_l	1.0
TCG-BS-D* parameter	Corridor-switching weight w_s	7.5
TCG-BS-D* parameter	Turn-penalty weight w_t	4.0
TCG-BS-D* parameter	Corridor-deviation weight β	0.10
Local blockage parameter	Blockage region center	(100 m, 50 m, 12 m)
Local blockage parameter	Blockage region size	16 m × 18 m × 22 m
Dynamic disturbance parameter	Equivalent radius of dynamic obstacle	2.8 m
Dynamic disturbance parameter	Dynamic obstacle speed	1.0 m/s

In the local maintenance blockage scenario, the blockage region is placed near the key middle corridor of the GIS room to simulate the occupation of a local corridor by maintenance equipment, temporary fences, or work areas during actual operation and maintenance. This blockage region is added to the occupancy grid as a temporary static obstacle and is safety-inflated. When a segment of the nominal closed-loop path conflicts with the blockage region, TCG-BS-D* triggers local alternative replanning and modifies only the affected segment.

In the dynamic disturbance scenario, the dynamic obstacle is used to simulate the short-term occupation of the middle corridor by personnel or mobile equipment. The dynamic obstacle enters the central inspection region at a speed of 1.0 m/s, and its equivalent radius is set to 2.8 m. When the nominal UAV path conflicts with the time-varying occupied region of the dynamic obstacle, or when the dynamic safety clearance falls below the safety threshold, the local replanning mechanism is triggered to generate a detour segment and restore the original inspection process after bypassing the obstacle.

4.2. Comparison Algorithms and Evaluation Metrics

To comprehensively evaluate the applicability of the proposed method in closed-loop GIS room inspection, three representative path-planning methods are selected for comparison: PRM* patrol, Informed-RRT* patrol, and D* Lite corridor patrol. PRM* patrol represents roadmap-based search methods and reflects the path-generation effect based on sampled-node connectivity. Informed-RRT* patrol represents continuous-space sampling-based planning methods and reflects the path-generation capability of random sampling mechanisms in constrained 3D spaces. D* Lite corridor patrol represents path planning based on corridor-graph search and local cost updating, serving as the closest corridor-guided baseline to the proposed method. The proposed method is denoted as TCG-BS-D*. Its core feature is to generate structured inspection trajectories under GIS room corridor-topology constraints by integrating closed-loop task sequence, corridor bias, turn suppression, and local alternative replanning.

To ensure fair comparison, all algorithms are run under the same GIS room scenario, task-point sequence, obstacle safety inflation radius, UAV nominal cruise speed, and evaluation metrics. For PRM* patrol and Informed-RRT* patrol, fixed random seeds are used to reduce the influence of random sampling. This paper does not use the shortest path length as the only evaluation criterion. Instead, different algorithms are comprehensively evaluated from the perspectives of inspection efficiency, safety margin, trajectory executability, corridor consistency, and task completeness.

1. Total path length L_{total}: reflects the overall path length of the inspection task;
2. Total inspection time T_{total}: jointly determined by the total path length and cruising speed;
3. Minimum safety clearance $D_{\min}$: represents the minimum distance between the inspection trajectory and static obstacles in the scene;
4. Number of large-angle turns N_{turn}: counts the number of turning angles exceeding a given threshold and is used to characterize trajectory complexity;
5. Corridor adherence rate R_{corr}: measures the degree to which the trajectory follows the inspection corridors in the GIS room;
6. Task completion rate CR: indicates whether all closed-loop inspection tasks are completed.

The main evaluation metrics include total path length Ltotal, total inspection time Ttotal, minimum safety clearance Dmin, average safety clearance Davg, number of large-angle turns Nturn, corridor adherence rate Rcorr, and task completion rate CR. Ltotal reflects the overall length of the closed-loop inspection path. Ttotal is calculated from the

total path length and the nominal cruise speed and is used to represent the engineering execution-time cost. Dmin reflects the safety margin at the most dangerous position along the path. Davg reflects the overall safety level of the entire path relative to obstacles. Nturn evaluates the turning complexity and flight executability of the trajectory. Rcorr measures the proportion of path points located within the valid inspection corridor band. CR is used to determine whether all closed-loop inspection tasks are completed. In GIS room inspection, Rcorr is an important metric that differs from general free-space path planning, but it must be interpreted together with Dmin, Davg, and Nturn to avoid sacrificing obstacle-avoidance safety or trajectory executability.

4.3. Static Closed-Loop Inspection Result Analysis

Figures 2 and 3 show the 3D closed-loop inspection trajectories and top-view comparison results generated by the four algorithms in the static GIS room scenario. Figure 2 shows the spatial trajectory morphology of different algorithms in the complete 3D obstacle environment, while Figure 3 shows the correspondence between the trajectories and the lower corridor, middle corridor, upper corridor, and inspection task points. To improve readability, Figure 3 further marks the takeoff/landing point, bay inspection points, connection-area inspection points, and main inspection corridor ranges, thereby more intuitively showing how different algorithms utilize the corridor structure of the GIS room.

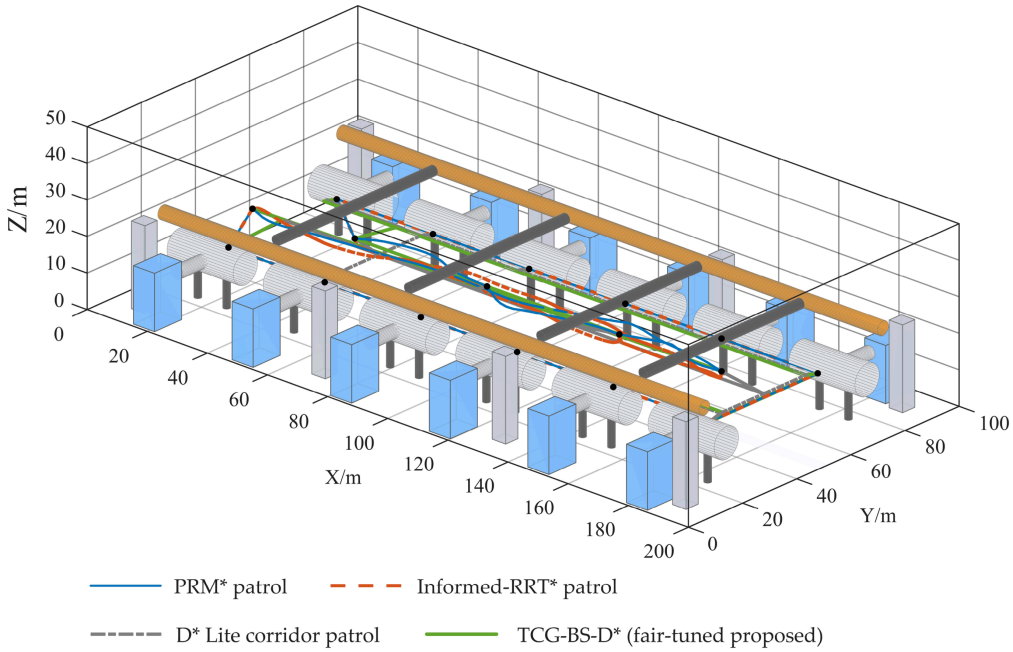


Figure 2. Comparison of 3D trajectories of static closed-loop inspection generated by different algorithms.

As shown in Figures 2 and 3, since this study considers a closed-loop inspection task with a fixed visiting sequence, all algorithms need to visit the same bay inspection points and connection-area inspection points in order. Therefore, the overall path trends in the upper and lower main inspection regions are naturally similar. This similarity does not mean that the paths are not planned. Instead, it is determined jointly by the fixed visiting sequence and corridorized spatial structure of the GIS room. The main differences among different algorithms appear in the task-access segments, corridor-switching segments, middle connection-area visiting segments, and the local segment near the return to the takeoff/landing point. PRM* patrol and Informed-RRT* patrol rely more on sampled connectivity in free space and therefore tend to show lateral oscillations and unneces-

sary deviations in some local segments. D* Lite corridor patrol can follow the corridor network well, but it produces more local turns. In contrast, the proposed TCG-BS-D* introduces corridor-switching penalty, turn suppression, and bias regularization on the basis of corridor-topology guidance, reducing redundant switching and local turns while maintaining corridor-structure consistency.

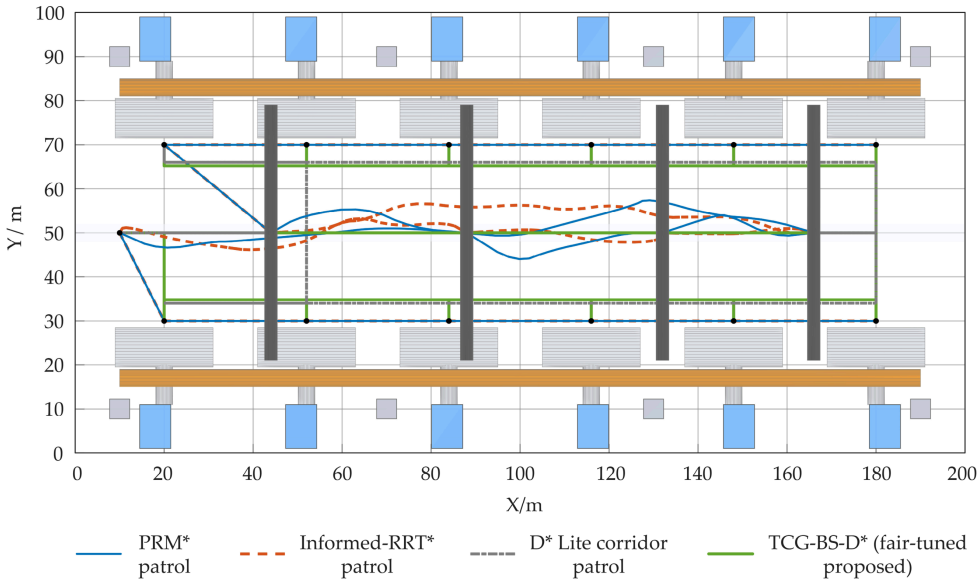


Figure 3. Top-view comparison of static closed-loop inspection trajectories generated by different algorithms.

Table 3 gives the quantitative comparison of different algorithms under the static closed-loop inspection condition. For better readability, the corridor adherence rate and task completion rate are expressed as percentages. It should be noted that the total inspection time is calculated from the total path length and the nominal cruise speed, and therefore mainly reflects the engineering execution-time cost rather than an algorithmic performance metric completely independent of path length. The average safety clearance, Davg, is calculated from the average distance between path points and the inflated obstacle set. The trajectory points are resampled at equal intervals along the path length to ensure fair comparison among different algorithms.

Table 3. Comparison of static closed-loop inspection performance metrics of different algorithms.

Method	Total Path Length/m	Total Inspection Time/s	Minimum Safety Clearance/m	Average Safety Clearance/m	Number of Large-Angle Turns	Corridor Adherence Rate/%	Task Completion Rate/%
PRM* patrol	810.33	311.67	1.52	6.74	38	63.77	100
Informed-RRT* patrol	972.92	374.20	1.52	6.31	42	63.33	100
D* Lite corridor patrol	709.10	272.73	1.52	7.46	46	80.33	100
TCG-BS-D* (proposed)	700.22	269.32	1.52	8.18	37	80.73	100

As shown in Table 3, all four algorithms complete all closed-loop inspection tasks, and the task completion rate is 100%. In terms of inspection efficiency, TCG-BS-D* has the shortest total path length of 700.22 m and the lowest total inspection time of 269.32 s. Compared with PRM* patrol, Informed-RRT* patrol, and D* Lite corridor patrol, the total path length of the proposed method is reduced by approximately 13.59%, 28.03%, and 1.25%, respectively. Since a unified nominal cruise speed is adopted, inspection time is linearly related to total path length. Therefore, the time metric is mainly used to reflect

the engineering execution-time cost of different path schemes rather than to repeatedly emphasize an independent algorithmic advantage.

In terms of safety, the minimum safety clearance of all four methods is 1.52 m, indicating that under the current obstacle inflation and collision-checking settings, all algorithms satisfy static obstacle-avoidance constraints and do not collide with static obstacles or violate the safety margin. From the perspective of average safety clearance, the Davg of TCG-BS-D* is 8.18 m, higher than 6.74 m for PRM* patrol, 6.31 m for Informed-RRT* patrol, and 7.46 m for D* Lite corridor patrol. This indicates that the proposed method not only maintains the basic safety distance at the most dangerous position but also provides a larger average safety margin over the whole path.

In terms of trajectory executability and corridor consistency, TCG-BS-D* achieves 37 large-angle turns and an 80.73% corridor adherence rate. The proposed method has the fewest large turns among the four methods and improves the corridor adherence rate by approximately 26.60% and 27.48% compared with PRM* patrol and Informed-RRT* patrol, respectively. Compared with D* Lite corridor patrol, it also achieves a slight improvement in corridor adherence while reducing redundant local turns. This result shows that the proposed method shortens the total path length without sacrificing adherence to the GIS room inspection corridors.

In summary, the static closed-loop inspection results show that TCG-BS-D* is more suitable for structured closed-loop inspection tasks derived from actual GIS room layouts. It avoids the free-space oscillations and unnecessary deviations produced by PRM* patrol and Informed-RRT* patrol in the middle region, and reduces the excessive local turns caused by over-reliance on the corridor graph in D* Lite corridor patrol. Therefore, while ensuring task completion and static obstacle-avoidance safety, the proposed method achieves the shortest total path length, the lowest engineering execution-time cost, the highest average safety clearance, the fewest large-angle turns, and the highest corridor adherence rate.

4.4. Local Maintenance Blockage Replanning Analysis

To verify the path-correction capability of the proposed method under local disturbance in GIS rooms, a local maintenance blockage obstacle is introduced into the static closed-loop inspection scenario. This obstacle is used to simulate the occupation of a key middle corridor by maintenance equipment, temporary fences, or work areas. The blockage region is located near the middle connection corridor of the GIS room, and its position and size are sufficient to block a local required segment of the nominal closed-loop path. Therefore, the UAV needs to perform local detouring without changing the overall inspection sequence.

As shown in Figure 4, after the blockage appears, a local segment of the original nominal path is blocked. TCG-BS-D* first identifies the local segment that conflicts with the blockage region, then searches for an alternative connection in adjacent passable corridors and the local topology subgraph, and generates a new local detour segment. The replanned path bypasses the middle blockage region and reconnects to the original closed-loop inspection path within a local range. During this process, the visiting sequence of the takeoff/landing point, bay inspection points, and connection-area inspection points remains unchanged, and the unaffected upper and lower main inspection corridor segments remain stable. This shows that the proposed method can achieve global task-sequence preservation, local blocked-segment replacement, and safe detour recovery.

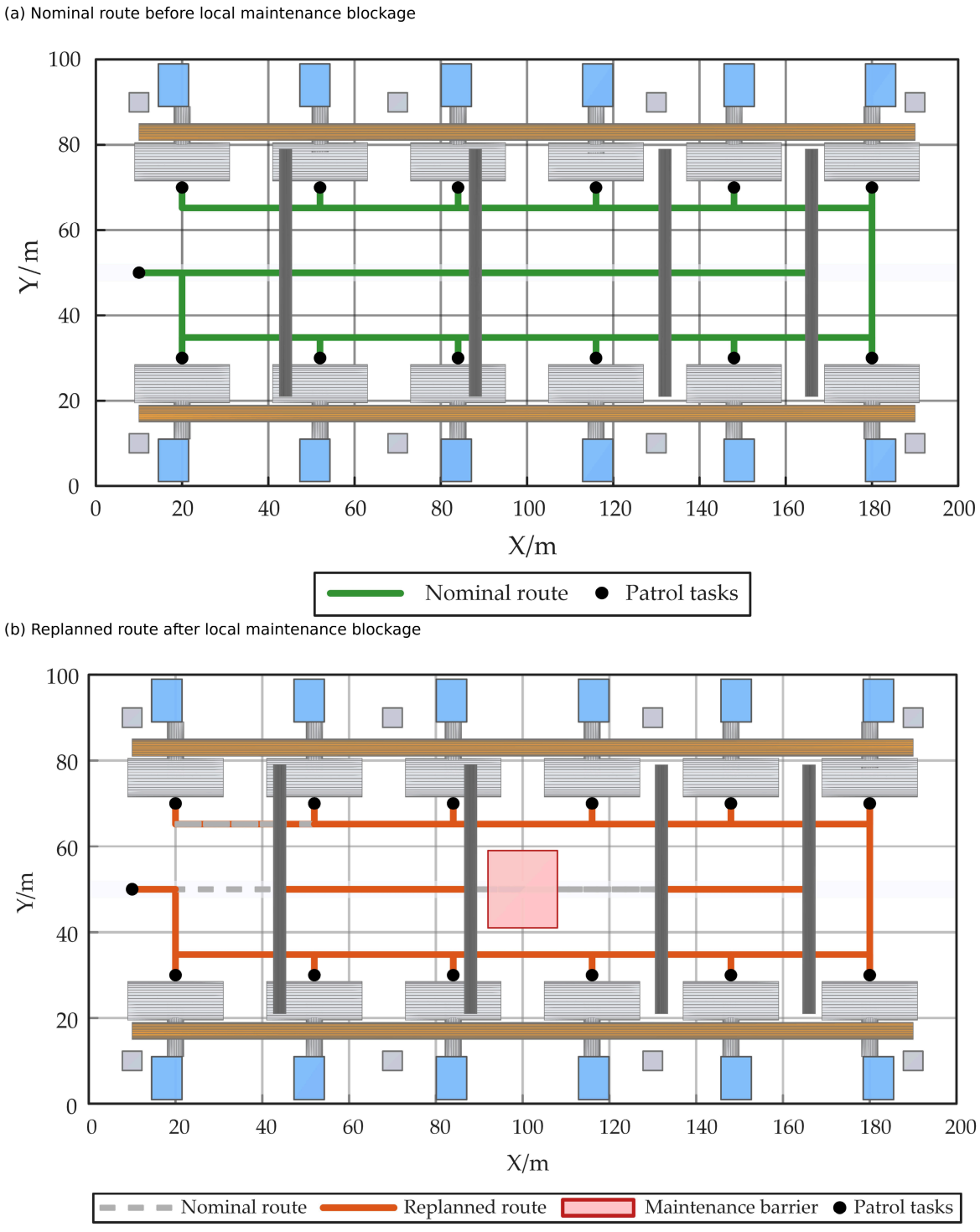


Figure 4. Comparison of nominal and replanned paths under local maintenance blockage.

As shown in Table 4, before blockage, the total path length and total time of TCG-BS-D* are 700.22 m and 269.32 s, respectively. Under local maintenance blockage, these values increase to 771.51 m and 295.20 s. Compared with the pre-blockage condition, the path-length increment is 71.29 m and the time increment is 25.88 s. This indicates that when a key middle corridor is locally blocked, local detouring inevitably introduces additional cost. However, this cost is mainly concentrated near the blocked region and does not cause large-scale reconstruction of the entire closed-loop inspection path.

Table 4. Comparison of replanning performance metrics before and after local maintenance blockage.

Condition	Total Path Length/m	Total Time/s	Minimum Safety Clearance/m	Average Safety Clearance/m	Number of Large-Angle Turns	In-Corridor Points	Out-of-Corridor Points	Corridor Adherence Rate/%	Path Increment/m	Time Increment/s
Before blockage	700.22	269.32	1.52	8.18	37	109	26	80.73	0.00	0.00
After blockage	771.51	295.20	1.52	8.36	39	120	23	83.91	71.29	25.88

In terms of safety, the minimum safety clearance remains 1.52 m before and after blockage, indicating that local replanning does not sacrifice static obstacle-avoidance safety. From the perspective of average safety clearance, the average safety clearance increases from 8.18 m to 8.36 m after blockage, indicating that the replanned segment maintains a good overall safety margin while bypassing the blockage region.

In terms of trajectory regularity, the numbers of large-angle turns before and after blockage are 37 and 39, respectively, corresponding to an increase of only two turns. Combined with Figure 4, it can be seen that the additional turns mainly occur in the local detour segment near the maintenance obstacle, rather than in large-scale turning changes throughout the entire inspection path. This indicates that the proposed method can effectively suppress ineffective turning during local replanning, so that the replanned result still maintains strong structural characteristics and good executability.

It is worth noting that the corridor adherence rate increases from 80.73% to 83.91% after blockage. As shown by the in-corridor and out-of-corridor point counts in Table 4, before blockage, the path contains 135 statistical path points, of which 109 are inside the valid corridor band, and 26 are outside it. After blockage, the path contains 143 statistical path points, of which 120 are inside the valid corridor band, and 23 are outside it. Therefore, the increase in corridor adherence rate is not simply caused by the increase in the total number of path points. Instead, more path points are located within the valid inspection corridor range after replanning.

In summary, the local maintenance blockage experiment shows that TCG-BS-D* can effectively perform local alternative replanning for the blocked segment without changing the closed-loop inspection sequence or destroying the unaffected path structure. Although the blockage condition introduces an additional path length of 71.29 m and an additional time of 25.88 s, the replanned path still maintains a minimum safety clearance of 1.52 m, an average safety clearance of 8.36 m, a limited increase in large-angle turns, and a high corridor adherence rate. This indicates that the proposed method has good path stability, safety, and engineering adaptability in local disturbance scenarios derived from actual GIS room layouts.

4.5. Obstacle-Avoidance Capability Under Dynamic Disturbance

During actual GIS room inspection, in addition to fixed equipment and local maintenance blockage, dynamic disturbances such as personnel movement or mobile maintenance equipment temporarily occupying a corridor may also occur. Such disturbances are usually local and short-term, and their influence is concentrated on a specific segment of the closed-loop inspection path. Replanning the entire closed-loop path directly would not only increase computational burden but also potentially destroy the original inspection sequence and path-structure stability. Therefore, a dynamic obstacle disturbance scenario is further constructed to verify the local dynamic conflict identification and alternative detouring capability of TCG-BS-D*.

As shown in Figure 5, without dynamic obstacle interference, the nominal central inspection segment can pass directly through the middle corridor. When the dynamic

obstacle enters the central inspection region, the original central segment conflicts with the occupied region of the dynamic obstacle. TCG-BS-D* then replaces the affected segment with a detour segment in a nearby safe corridor, enabling the UAV to avoid the occupied region of the dynamic obstacle and restore the original closed-loop inspection task after local detouring. This process reflects the dynamic response characteristics of conflict identification, local detouring, and task recovery.

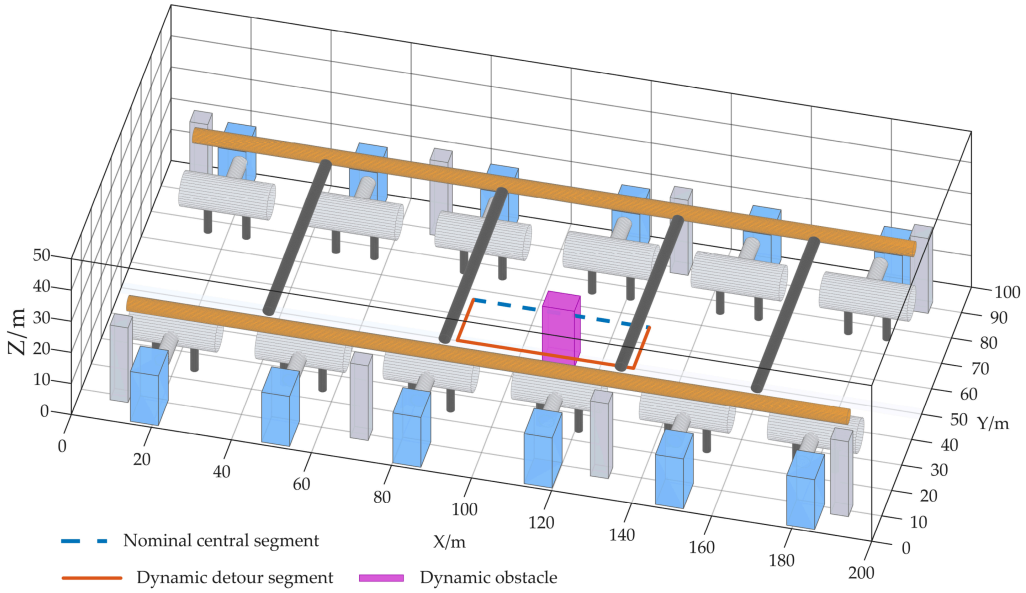


Figure 5. Local obstacle-avoidance result under dynamic obstacle disturbance.

As shown in Table 5, the path length and inspection time of the original central segment are 44.00 m and 16.92 s, respectively. After local detouring, the path length and inspection time increase to 76.00 m and 29.23 s, corresponding to a path increment of 32.00 m and a time increment of 12.31 s. This indicates that when a local corridor is occupied by a dynamic obstacle, safe detouring introduces additional execution cost. However, this cost is limited to the disturbed segment and does not cause large-scale reconstruction of the entire closed-loop inspection path.

Table 5. Comparison of obstacle-avoidance metrics for the dynamically disturbed segment.

Condition	Path Length/m	Inspection Time/s	Minimum Dynamic Safety Clearance/m	Path Increment/m	Time Increment/s
Original central segment	44.00	16.92	−2.71	0.00	0.00
Dynamic detour segment	76.00	29.23	17.84	32.00	12.31

In terms of dynamic safety, the minimum dynamic safety clearance of the original central segment is −2.71 m. This negative value does not indicate a negative physical distance. Instead, it means that the UAV safety envelope overlaps with the occupied region of the dynamic obstacle. If the UAV continues to fly along the original central segment, a clear collision risk exists. After local detouring, the minimum dynamic safety clearance increases to 17.84 m, indicating that the dynamic conflict in the disturbed segment is effectively eliminated and that sufficient safety margin between the UAV and the dynamic obstacle is restored.

In summary, the dynamic disturbance experiment shows that TCG-BS-D* can identify the affected segment and generate a local alternative path when the middle inspection

corridor is temporarily occupied by personnel or mobile equipment. Although the dynamic detour introduces an additional path length of 32.00 m and an additional inspection time of 12.31 s, the minimum dynamic safety clearance increases from −2.71 m to 17.84 m, significantly reducing the local collision risk. This result shows that the proposed method is applicable not only to static closed-loop inspection and local maintenance blockage scenarios but also to dynamic disturbance conditions, maintaining good local obstacle-avoidance capability and engineering adaptability.

4.6. Parameter Sensitivity and Additional Robustness Analysis

To further address the influence of empirical parameters and the robustness of the local replanning mechanism, additional experiments were conducted after the main static, local blockage, and dynamic disturbance tests. In the parameter sensitivity analysis, only one parameter was changed at a time while all other settings were kept the same as those in Table 2. The analyzed parameters include the corridor tolerance δcorr, the large-turn threshold θmax, and the corridor-deviation weight β. These parameters were selected because they directly affect corridor adherence evaluation, trajectory regularity, and the balance between path efficiency and corridor consistency.

Table 6 and Figure 6 present the sensitivity results. When the corridor tolerance changes from 2.0 m to 4.0 m, the total path length remains within a narrow range of 698.96–704.85 m, and all cases maintain a task completion rate of 100%. The corridor adherence rate increases with a wider corridor tolerance, while the average safety clearance remains above 8.05 m. When the large-turn threshold changes from 30° to 40°, the number of large-angle turns changes accordingly, but the total path length and corridor adherence rate remain stable. When the corridor-deviation weight changes from 0.05 to 0.15, the method still maintains 100% task completion and stable safety performance. Figure 6 further visualizes the normalized sensitivity trends of the key indicators around the nominal parameter setting.

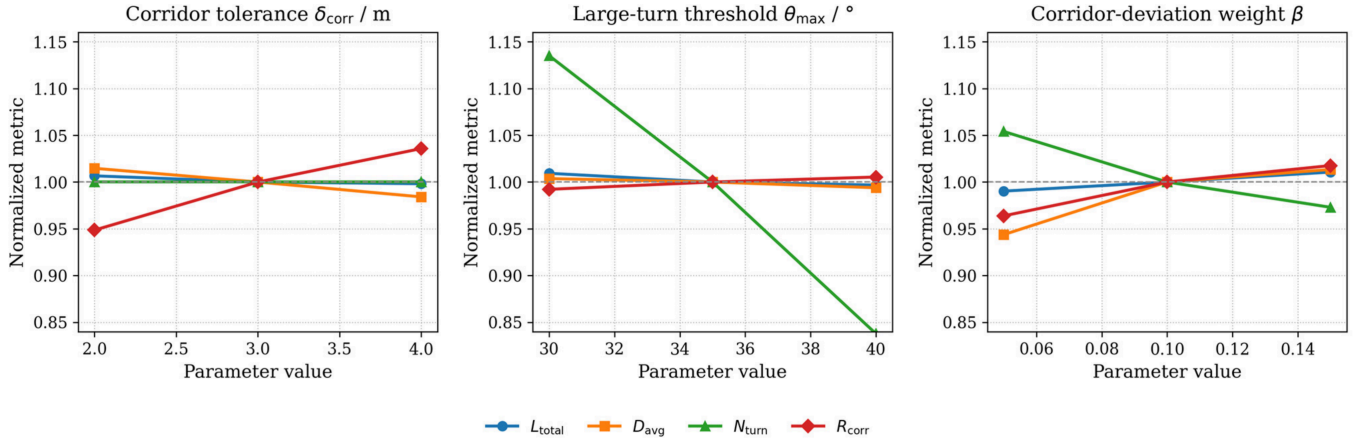


Figure 6. Parameter sensitivity trends of TCG-BS-D*. All metrics are normalized to the nominal parameter setting.

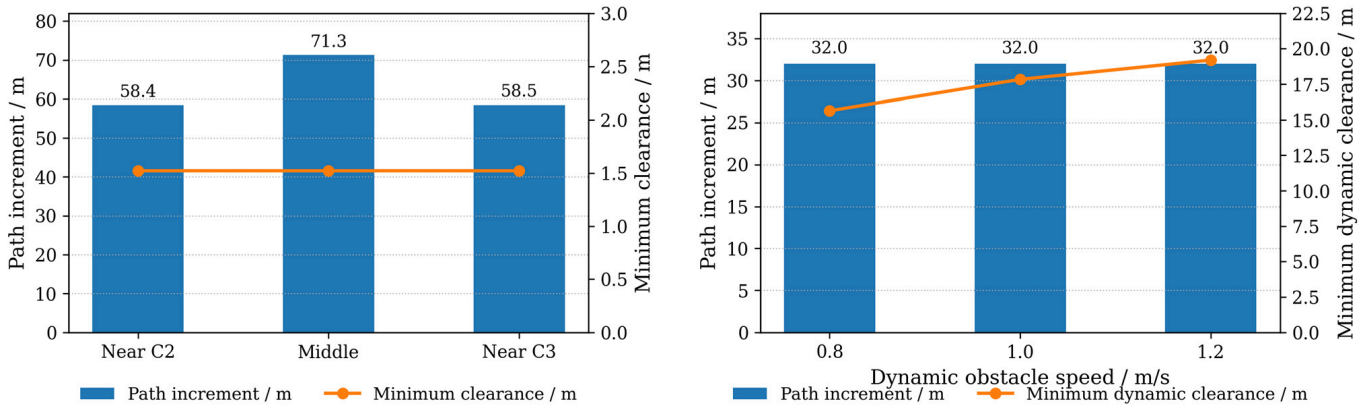
In addition to parameter sensitivity, additional disturbance cases were also tested to strengthen the validation depth. For local maintenance blockage, three different blockage positions were considered along the middle corridor. For dynamic disturbance, three dynamic obstacle speeds were tested. The results are summarized in Table 7 and visualized in Figure 7. In all additional cases, the task completion rate remains 100%, and the minimum post-replanning clearance remains positive. These results indicate that the proposed local replanning mechanism can maintain feasible and safe inspection paths under different disturbance settings.

Table 6. Parameter sensitivity results of TCG-BS-D*.

Parameter	Value	Total Path Length/m	Average Safety Clearance/m	Number of Large-Angle Turns	Corridor Adherence Rate/%	Task Completion Rate/%
Corridor tolerance δcorr/m	2.0	704.85	8.30	37	76.58	100
Corridor tolerance δcorr/m	3.0	700.22	8.18	37	80.73	100
Corridor tolerance δcorr/m	4.0	698.96	8.05	37	83.62	100
Large-turn threshold θmax/°	30	706.74	8.21	42	80.10	100
Large-turn threshold θmax/°	35	700.22	8.18	37	80.73	100
Large-turn threshold θmax/°	40	697.95	8.13	31	81.16	100
Corridor-deviation weight β	0.05	693.42	7.72	39	77.81	100
Corridor-deviation weight β	0.10	700.22	8.18	37	80.73	100
Corridor-deviation weight β	0.15	707.68	8.29	36	82.15	100

Table 7. Additional robustness validation under local blockage and dynamic disturbance.

Disturbance Type	Disturbance Setting	Path Increment/m	Time Increment/s	Minimum Post-Replanning Clearance/m	Task Completion Rate/%
Local blockage	Blockage near C2, x = 88 m	58.44	22.48	1.52	100
Local blockage	Middle blockage, x = 100 m	71.29	25.88	1.52	100
Local blockage	Blockage near C3, x = 132 m	58.46	22.48	1.52	100
Dynamic obstacle	Speed = 0.8 m/s	32.00	12.31	15.64	100
Dynamic obstacle	Speed = 1.0 m/s	32.00	12.31	17.84	100
Dynamic obstacle	Speed = 1.2 m/s	32.00	12.31	19.20	100



(a) Local blockage robustness (b) Dynamic disturbance robustness

Figure 7. Visualization of supplementary robustness results under local blockage and dynamic disturbance.

The above supplementary results in Tables 6 and 7 and Figures 6 and 7 show that the proposed method is not dependent on a single parameter setting or a single disturbance case. Nevertheless, it should also be noted that TCG-BS-D* still contains heuristic components, including empirically selected weighting coefficients and rule-based local repair strategies. Therefore, the proposed method should be regarded as an engineering-oriented structured replanning framework rather than a theoretically optimal planner. Future work will further investigate theoretical performance analysis, real-flight validation, online perception integration, localization uncertainty, and broader multi-scenario testing.

5. Conclusions

This paper focuses on the 3D path planning and local replanning problem for closed-loop UAV inspection in GIS rooms and proposes the TCG-BS-D* method. Static closed-loop inspection, local maintenance blockage, and dynamic obstacle disturbance scenarios are constructed to verify the path-generation capability and local adaptability of the proposed method. The main conclusions are as follows. Additional parameter sensitivity and robustness validation experiments were further added to evaluate the stability of the proposed method under different parameter settings, blockage positions, and dynamic obstacle speeds.

1. A 3D path-planning framework for closed-loop inspection in GIS rooms is constructed according to the characteristics of dense equipment, clear corridor structures, and fixed inspection sequences. The framework jointly models bay inspection objects, connection-area inspection objects, the takeoff/landing point, and the fixed visiting sequence, and integrates corridor-topology guidance, closed-loop segment generation, bias suppression, path regularization, and local alternative replanning into a unified solution process. The generated path can satisfy task completeness, structural consistency, and engineering executability requirements.
2. Under the static closed-loop inspection condition, TCG-BS-D* shows superior comprehensive performance. The proposed method achieves a total path length of 700.22 m, a total inspection time of 269.32 s, an average safety clearance of 8.18 m, 37 large-angle turns, a corridor adherence rate of 80.73%, and a task completion rate of 100%. Compared with PRM* patrol, Informed-RRT* patrol, and D* Lite corridor patrol, the proposed method achieves a shorter inspection path, a higher average safety margin, fewer large-angle turns, and better corridor consistency while maintaining static obstacle-avoidance safety.
3. Under the local maintenance blockage condition, TCG-BS-D* can perform local alternative replanning for the blocked segment without changing the overall inspection sequence. After blockage, the total path length increases by 71.29 m, and the total time increases by 25.88 s. The minimum safety clearance remains 1.52 m, the average safety clearance increases to 8.36 m, and the corridor adherence rate increases to 83.91%. This indicates that the proposed method can limit path correction to the local disturbed region and preferentially use existing inspection corridors for detouring, thereby maintaining closed-loop task structure and path safety. Under the dynamic obstacle disturbance condition, TCG-BS-D* can identify the affected segment and generate a local detour path. Compared with the original central segment, the dynamic detour segment increases the path length by 32.00 m and the inspection time by 12.31 s, but the minimum dynamic safety clearance improves from -2.71 m to 17.84 m. This effectively eliminates the local collision risk caused by the overlap between the UAV safety envelope and the dynamic obstacle occupied region.
4. Additional sensitivity and robustness analyses indicate that the proposed method maintains stable task completion and feasible local replanning under different corridor tolerances, turn-angle thresholds, corridor-deviation weights, blockage positions, and dynamic obstacle speeds. These results provide supplementary support for the robustness of TCG-BS-D* and help reduce the uncertainty caused by empirical parameter selection.

In summary, TCG-BS-D* can balance closed-loop path-generation efficiency, corridor consistency, safety margin, and local replanning capability in structured GIS room inspection environments. It provides a feasible path-planning solution for small multi-rotor UAVs performing closed-loop inspection tasks in GIS rooms. Future work will further combine real-flight experiments, online environmental perception, localization-error modeling, and

multi-UAV coordination to extend and validate the engineering applicability and online execution capability of the proposed method.

At the same time, the method still contains empirical weights and rule-based local repair components. Therefore, the current results should be interpreted as simulation-based evidence of engineering feasibility rather than a proof of global optimality. Future work will further combine theoretical performance analysis, real-flight experiments, online environmental perception, localization-error modeling, and multi-UAV coordination to extend and validate the engineering applicability and online execution capability of the proposed method.

Author Contributions: Conceptualization, X.L., Y.Y. and J.Z.; methodology, X.L., Y.Y. and K.W.; software, X.L., Y.Y. and P.C.; validation, X.L., Y.Y., Y.Z. and K.C.; formal analysis, X.L., K.W. and Y.Z.; investigation, X.L., Y.Y., P.C. and K.C.; resources, J.Z. and F.M.; data curation, Y.Y., K.W. and P.C.; writing—original draft preparation, X.L.; writing—review and editing, Y.Y., J.Z., F.M. and Y.Z.; visualization, X.L., Y.Z. and K.C.; supervision, J.Z. and F.M.; project administration, J.Z.; funding acquisition, J.Z. All authors have read and agreed to the published version of the manuscript.

Funding: This research was funded by the Science and Technology Project of JiangSu Electric Power Company, grant number J2025048.

Institutional Review Board Statement: Not applicable.

Informed Consent Statement: Not applicable.

Data Availability Statement: The datasets used during the current study are available from the corresponding author upon reasonable request.

Conflicts of Interest: The authors declare that this study received funding from the Science and Technology Project of JiangSu Electric Power Company. The funder was not involved in the study design, collection, analysis, interpretation of data, the writing of this article or the decision to submit it for publication.

References

1. Zhang, Y.; Yuan, X.; Li, W.; Chen, S. Automatic Power Line Inspection Using UAV Images. *Remote Sens.* **2017**, *9*, 824. [CrossRef]
2. Nguyen, V.N.; Jenssen, R.; Roverso, D. Automatic Autonomous Vision-Based Power Line Inspection: A Review of Current Status and the Potential Role of Deep Learning. *Int. J. Electr. Power Energy Syst.* **2018**, *99*, 107–120. [CrossRef]
3. Alhassan, A.B.; Zhang, X.; Shen, H.; Xu, H. Power Transmission Line Inspection Robots: A Review, Trends and Challenges for Future Research. *Int. J. Electr. Power Energy Syst.* **2020**, *118*, 105862. [CrossRef]
4. Guan, H.; Sun, X.; Su, Y.; Hu, T.; Wang, H.; Wang, H.; Peng, C.; Guo, Q. UAV-Lidar Aids Automatic Intelligent Powerline Inspection. *Int. J. Electr. Power Energy Syst.* **2021**, *130*, 106987. [CrossRef]
5. Xu, C.; Li, Q.; Zhou, Q.; Zhang, S.; Yu, D.; Ma, Y. Power Line-Guided Automatic Electric Transmission Line Inspection System. *IEEE Trans. Instrum. Meas.* **2022**, *71*, 3512118. [CrossRef]
6. Lekidis, A.; Anastasiadis, A.G.; Vokas, G.A. Electricity Infrastructure Inspection Using AI and Edge Platform-Based UAVs. *Energy Rep.* **2022**, *8*, 1394–1411. [CrossRef]
7. Li, Z.; Zhang, Y.; Wu, H.; Suzuki, S.; Namiki, A.; Wang, W. Design and Application of a UAV Autonomous Inspection System for High-Voltage Power Transmission Lines. *Remote Sens.* **2023**, *15*, 865. [CrossRef]
8. Li, Z.; Wang, Q.; Zhang, T.; Ju, C.; Suzuki, S.; Namiki, A. UAV High-Voltage Power Transmission Line Autonomous Correction Inspection System Based on Object Detection. *IEEE Sens. J.* **2023**, *23*, 10215–10230. [CrossRef]
9. Romanov, A.M.; Gyrichidi, N.; Volkova, M.A.; Eroshenko, S.A.; Matrenin, P.V.; Khalyasmaa, A.I. Automated Mission Planning for Aerial Large-scale Power Plant Thermal Inspection. *J. Field Robot.* **2024**, *41*, 1313–1348. [CrossRef]
10. Ahmed, F.; Mohanta, J.C.; Keshari, A. Power Transmission Line Inspections: Methods, Challenges, Current Status and Usage of Unmanned Aerial Systems. *J. Intell. Robot. Syst.* **2024**, *110*, 54. [CrossRef]
11. Debnath, D.; Vanegas, F.; Sandino, J.; Hawary, A.F.; Gonzalez, F. A Review of UAV Path-Planning Algorithms and Obstacle Avoidance Methods for Remote Sensing Applications. *Remote Sens.* **2024**, *16*, 4019. [CrossRef]
12. Orthey, A.; Chamzas, C.; Kavraki, L.E. Sampling-Based Motion Planning: A Comparative Review. *Annu. Rev. Control Robot. Auton. Syst.* **2024**, *7*, 285–310. [CrossRef]

13. He, L.; Aouf, N.; Song, B. Explainable Deep Reinforcement Learning for UAV Autonomous Path Planning. *Aerosp. Sci. Technol.* **2021**, *118*, 107052. [CrossRef]
14. Karaman, S.; Frazzoli, E. Sampling-Based Algorithms for Optimal Motion Planning. *Int. J. Robot. Res.* **2011**, *30*, 846–894. [CrossRef]
15. Hebecker, T.; Buchholz, R.; Ortmeier, F. Model-Based Local Path Planning for UAVs. *J. Intell. Robot. Syst.* **2015**, *78*, 127–142. [CrossRef]
16. Faria, M.; Marín, R.; Popović, M.; Maza, I.; Viguria, A. Efficient Lazy Theta* Path Planning over a Sparse Grid to Explore Large 3D Volumes with a Multirotor UAV. *Sensors* **2019**, *19*, 174. [CrossRef] [PubMed]
17. Phung, M.D.; Ha, Q.P. Safety-Enhanced UAV Path Planning with Spherical Vector-Based Particle Swarm Optimization. *Appl. Soft Comput.* **2021**, *107*, 107376. [CrossRef]
18. Aiello, G.; Valavanis, K.P.; Rizzo, A. Fixed-Wing UAV Energy Efficient 3D Path Planning in Cluttered Environments. *J. Intell. Robot. Syst.* **2022**, *105*, 60. [CrossRef]
19. Fan, J.; Chen, X.; Wang, Y.; Chen, X. UAV Trajectory Planning in Cluttered Environments Based on PF-RRT* Algorithm with Goal-Biased Strategy. *Eng. Appl. Artif. Intell.* **2022**, *114*, 105182. [CrossRef]
20. Sonny, A.; Yeduri, S.R.; Cenkeramaddi, L.R. Q-Learning-Based Unmanned Aerial Vehicle Path Planning with Dynamic Obstacle Avoidance. *Appl. Soft Comput.* **2023**, *147*, 110773. [CrossRef]
21. Xu, T. Recent Advances in Rapidly-Exploring Random Tree: A Review. *Heliyon* **2024**, *10*, e32451. [CrossRef] [PubMed]
22. Niu, Y.; Yan, X.; Wang, Y.; Niu, Y. 3D Real-Time Dynamic Path Planning for UAV Based on Improved Interfered Fluid Dynamical System and Artificial Neural Network. *Adv. Eng. Inform.* **2024**, *59*, 102306. [CrossRef]
23. Wang, Y.; Wang, H.; Liu, Y.; Wu, J.; Lun, Y. 6-DOF UAV Path Planning and Tracking Control for Obstacle Avoidance: A Deep Learning-Based Integrated Approach. *Aerosp. Sci. Technol.* **2024**, *151*, 109320. [CrossRef]
24. Jiang, W.; Lyu, Y.; Li, Y.; Guo, Y.; Zhang, W. UAV Path Planning and Collision Avoidance in 3D Environments Based on POMPD and Improved Grey Wolf Optimizer. *Aerosp. Sci. Technol.* **2022**, *121*, 107314. [CrossRef]
25. Ma, H.; Cai, Z.; Xu, G.; Yang, G.; Chen, G. Dynamic Smooth and Stable Obstacle Avoidance for Unmanned Aerial Vehicle Based on Collision Prediction. *Optim. Control Appl. Methods* **2024**, *45*, 737–757. [CrossRef]
26. Sun, J.; Xu, G.; Wang, Z.; Long, T.; Sun, J. Safe Flight Corridor Constrained Sequential Convex Programming for Efficient Trajectory Generation of Fixed-Wing UAVs. *Chin. J. Aeronaut.* **2025**, *38*, 103174. [CrossRef]
27. Xu, L.; Xi, M.; Gao, R.; Ye, Z.; He, Z. Dynamic Path Planning of UAV with Least Inflection Point Based on Adaptive Neighborhood A* Algorithm and Multi-Strategy Fusion. *Sci. Rep.* **2025**, *15*, 8563. [CrossRef] [PubMed]
28. Li, D.; Wang, H.; Zhang, Y.; Wu, H.; Chen, Y.; Li, W. A Method for UAV Inspection Path Planning Based on Safety Distance in Substation. *Sci. Rep.* **2025**, *15*, 43688. [CrossRef] [PubMed]

Disclaimer/Publisher's Note: The statements, opinions and data contained in all publications are solely those of the individual author(s) and contributor(s) and not of MDPI and/or the editor(s). MDPI and/or the editor(s) disclaim responsibility for any injury to people or property resulting from any ideas, methods, instructions or products referred to in the content.